



HAL
open science

Enhancement of piezoelectric response in Ga doped BiFeO₃ epitaxial thin films

Nazir Jaber, Jérôme Wolfman, Christophe Daumont, Béatrice Negulescu,
Antoine Ruyter, Guy Feuillard, M. Bavencoffe, J. Fortineau, T. Sauvage, B.
Courtois, et al.

► **To cite this version:**

Nazir Jaber, Jérôme Wolfman, Christophe Daumont, Béatrice Negulescu, Antoine Ruyter, et al..
Enhancement of piezoelectric response in Ga doped BiFeO₃ epitaxial thin films. *Journal of Applied
Physics*, 2015, 117 (24), 10.1063/1.4923217 . hal-01741553

HAL Id: hal-01741553

<https://hal.science/hal-01741553>

Submitted on 21 Feb 2022

HAL is a multi-disciplinary open access archive for the deposit and dissemination of scientific research documents, whether they are published or not. The documents may come from teaching and research institutions in France or abroad, or from public or private research centers.

L'archive ouverte pluridisciplinaire **HAL**, est destinée au dépôt et à la diffusion de documents scientifiques de niveau recherche, publiés ou non, émanant des établissements d'enseignement et de recherche français ou étrangers, des laboratoires publics ou privés.

Enhancement of piezoelectric response in Ga doped BiFeO₃ epitaxial thin films

N. Jaber, J. Wolfman, C. Daumont, B. Négulescu, A. Ruyter, G. Feuillard, M. Bavencoffe, J. Fortineau, T. Sauvage, B. Courtois, H. Bouyanfif, J. L. Longuet, C. Autret-Lambert, and F. Gervais

Citation: [Journal of Applied Physics](#) **117**, 244107 (2015); doi: 10.1063/1.4923217

View online: <http://dx.doi.org/10.1063/1.4923217>

View Table of Contents: <http://scitation.aip.org/content/aip/journal/jap/117/24?ver=pdfcov>

Published by the [AIP Publishing](#)

Articles you may be interested in

[Ferroelectric polarization and defect-dipole switching in an epitaxial \(111\) BiFeO₃ thin film](#)

[J. Appl. Phys.](#) **117**, 204103 (2015); 10.1063/1.4921808

[Magnetic and structural properties of BiFeO₃ thin films grown epitaxially on SrTiO₃/Si substrates](#)

[J. Appl. Phys.](#) **113**, 17D919 (2013); 10.1063/1.4796150

[Direct piezoelectric properties of \(100\) and \(111\) BiFeO₃ epitaxial thin films](#)

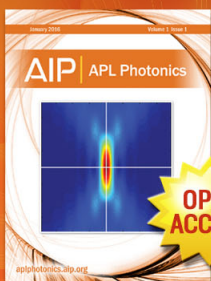
[Appl. Phys. Lett.](#) **100**, 102901 (2012); 10.1063/1.3692579

[Effect of bottom electrodes on nanoscale switching characteristics and piezoelectric response in polycrystalline BiFeO₃ thin films](#)

[J. Appl. Phys.](#) **110**, 084102 (2011); 10.1063/1.3651383

[Polarization switching in epitaxial Bi Fe O 3 films](#)

[Appl. Phys. Lett.](#) **87**, 252902 (2005); 10.1063/1.2149180



Launching in 2016!
The future of applied photonics research is here

AIP | APL
Photonics

Enhancement of piezoelectric response in Ga doped BiFeO₃ epitaxial thin films

N. Jaber,¹ J. Wolfman,^{1,a)} C. Daumont,¹ B. Négulescu,¹ A. Ruyter,¹ G. Feuillard,¹ M. Bavencoffe,¹ J. Fortineau,¹ T. Sauvage,² B. Courtois,² H. Bouyanfif,³ J. L. Longuet,⁴ C. Autret-Lambert,¹ and F. Gervais¹

¹Laboratoire GREMAN, UMR7347 CNRS, Faculté des sciences et techniques, Université François Rabelais, 37200 Tours, France

²Laboratoire CEMHTI, UPR3079 CNRS, Site Cyclotron 45071, Orléans cedex 2, France

³Laboratoire LPMC, Université Jules Verne Picardie-Amiens, Amiens, France

⁴CEA, DAM, Le Ripault, F-37260 Monts, France

(Received 13 May 2015; accepted 17 June 2015; published online 30 June 2015)

The piezoelectric properties of compositional spread $(1-x)\text{BiFeO}_3\text{-}x\text{GaFeO}_3$ epitaxial thin films are investigated where Ga³⁺ substitution for Bi³⁺ is attempted in $\text{Bi}_{1-x}\text{Ga}_x\text{FeO}_3$ compounds. Ga content x was varied from 0 to 12% (atomic). Ferroelectric characterizations are reported at various length scales. Around 6.5% of Ga content, an enhancement of the effective piezoelectric coefficient d_{33}^{eff} is observed together with a change of symmetry of the film. Measured d_{33}^{eff} values in 135 nm thick films increased from 25 pm/V for undoped BiFeO₃ to 55 pm/V for 6.5% Ga with no extrinsic contribution from ferroelastic domain rearrangement. © 2015 AIP Publishing LLC.

[<http://dx.doi.org/10.1063/1.4923217>]

I. INTRODUCTION

Most microelectromechanical systems (MEMS) used for sensing, actuating, or energy harvesting applications incorporate $(1-x)\text{PbZrO}_3\text{-}x\text{PbTiO}_3$ (PZT) ferroelectric films as piezoelectric transducers, because their large piezoelectric coefficients and electromechanical coupling enable long range motions and high energy densities.¹ Relaxor-ferroelectrics like $(1-x)\text{PbMg}_{1/3}\text{Nb}_{2/3}\text{O}_3\text{-}x\text{PbTiO}_3$ (PMN-xPT) exhibit even better piezoelectric properties than PZT and are considered as possible next generation transducers.² A unique characteristic of solid solutions like PZT or PMN-xPT is the noticeable enhancement of their piezoelectric coefficients in the vicinity of a composition induced phase transition called morphotropic phase boundary (MPB). In the case of PZT, the MPB lies between a rhombohedral ferroelectric phase and a tetragonal ferroelectric phase,³ while in the case of PMN-xPT, it lies between a relaxor pseudo-cubic phase and a ferroelectric tetragonal phase.⁴ We note in the latter case that near the MPB, the pseudo cubic relaxor phase turns into a rhombohedral ferroelectric phase upon poling. The microscopic origin of this enhanced piezoelectric activity is still being debated but usually involves easiness of polarization rotation at the MPBs.^{2,5-7} Another common feature of these solid solutions is that they are lead-based and thus targeted by environmental regulations like the Restriction on Hazardous Substances (RoHS) EU Directive. Thus, alternative piezoelectric lead-free materials are required, and an obvious direction is to look for MPBs in other ferroelectric solid solutions.

Bismuth ferrite BiFeO₃ (BFO) being a ferroelectric ($T_c \sim 1100\text{ K}$ (Refs. 8 and 9)) with record polarization ($100\ \mu\text{C}\cdot\text{cm}^{-2}$) and having a rhombohedrically distorted perovskite structure (SG R3c^{10,11}) is a good starting point. As

BFO is also antiferromagnetic ($T_N \sim 643\text{ K}$ (Ref. 12)), it has recently attracted a lot of attention for its unique room-temperature combination of multiferroic properties.¹³ Solid-solutions of BFO with tetragonal ferroelectric perovskite phase like PbTiO₃ and BaTiO₃ have been synthesized, and MPBs have been found in both cases around 70% of BFO. In BFO- $x\text{BaTiO}_3$, a transition from a rhombohedral ferroelectric to a pseudo-cubic relaxor (PMN-xPT-like) is associated with a strong increase of d_{33} (up to 140 pm/V).¹⁴ In BFO- $x\text{PbTiO}_3$, the MPB separates rhombohedral and tetragonal ferroelectric phases (PZT-like),¹⁵ but the low resistivity of the resulting compounds prevented from obtaining high d_{33} values.¹⁶ However, it was shown that MPBs could also be induced by pressure,⁵ epitaxial strain,¹⁷ electric field,¹⁸⁻²¹ temperature,¹⁸ and/or chemical substitution.^{21,22} In particular, chemical substitution allows for the search of new systems for which the end member of the phase diagram does not need to be a ferroelectric crystallizing in the perovskite structure. Indeed, even though BiGaO₃ (BGO) crystallizes in a pyroxene-type structure, it has recently been reported that the $(1-x)\text{BFO-}x\text{BGO}$ system exhibits a perovskite structure for $x < 0.6$. Moreover, there is a region where Cm and R3c symmetries coexist ($0.2 \leq x \leq 0.3$)²³ that could be the host for a MPB. The ferroelectric properties of this system were later investigated under thin film form and have shown enhanced polarization (up to $230\ \mu\text{C}\cdot\text{cm}^{-2}$) (Refs. 24 and 25), but no quantitative data on its piezoelectric properties are available nowadays. In this paper, we report on the piezoelectric properties enhancement of Ga doped BFO films using another substitution scheme in the system $(1-x)\text{BFO-}x\text{GaFeO}_3$.

II. EXPERIMENTAL DETAILS

Composition spread Ga-doped BFO epitaxial films (BGFO) were grown by combinatorial pulsed laser deposition

^{a)}E-mail: wolfman@univ-tours.fr

(PLD) on (001)-oriented SrTiO₃ single crystals using a KrF excimer (248 nm).²⁶ A basic cycle of serial deposition from Bi_{1-x}FeO₃ and GaFeO₃ targets for the growth of about 1 nm thick alloyed films is repeated hundreds of times. A mobile mask close to the substrate controls the composition gradient along one direction of the sample while keeping the composition constant along the perpendicular direction. The Bi over stoichiometry of BFO target compensates for the Bi volatility and allows the stabilization of monophasic BFO films. GaFeO₃ (GFO) does not have a perovskite structure but crystallizes in an orthorhombic structure (SG P₂n), where the Ga³⁺ and Fe³⁺ cations are randomly distributed on four sites.²⁷ Furthermore, GFO is ferrimagnetic, piezoelectric,^{28,29} and was recently shown to be weakly ferroelectric (T_N ~ 150 K).³⁰ In the (1-x)BFO-(x)GFO system designed here, Ga³⁺ cations have incentives to substitute for Bi³⁺. Small ions like Ga³⁺ (ionic radius r_{VI} = 62 pm) do not occupy perovskite A-site in conventionally synthesized ceramics. However, perovskites with small A-site cations like Sc³⁺ (r_{VI} = 74.5 pm) and Mg²⁺ (r_{VI} = 72 pm) have recently been stabilized using high-pressure high-temperature synthesis, and both Ga³⁺ and Al³⁺ are envisaged as A-site cations in this emerging field.³¹ Epitaxial strain during PLD growth has longtime proven to be an alternative to high pressure synthesis for metastable phase stabilization.³² Furthermore, the Goldsmith tolerance factor *t* corresponding to the range of Ga³⁺ substitution studied here (0% ≤ *x* ≤ 12%) is greater than 0.87, not too far from non-substituted BFO's tolerance factor (*t* = 0.89), and compatible with a distorted perovskite structure. So, it is plausible that some Ga³⁺ ions occupy the perovskite A-site in our films, although it is probable too that part of the Ga³⁺ shares the B-site together with Fe³⁺.

BGFO films were deposited onto a 50 nm thick La_{0.8}Sr_{0.2}MnO₃ (LSMO) bottom electrode. The growth was performed at a substrate temperature of 700 °C in a dynamic oxygen pressure of 2.10⁻¹ mbar. The laser fluence and repetition rates were set at 1.72 J/cm² and 6 Hz for Bi_{1-x}FeO₃ and GFO and at 0.48 J/cm² and 4 Hz for LSMO. After deposition, the films were cooled down to room temperature at 3 °C/min in 500 mbar of static oxygen pressure. The concentration variation of Ga across the spread was characterized by Wavelength Dispersive X-ray Spectroscopy on an Electron Probe MicroAnalyser equipped with four WDS spectrometers (WDS-EPMA SX50, Cameca). Due to the layered structure of the sample, a specific thin film analysis (TFA/WDS) program has to be used to determine the correct composition of the BGFO-*x* top layer (layerf, Cameca). Analysis was performed with various incident electron beam energy (from 8 to 20 keV). Probe current was relatively high (100 to 200 nA) to detect low Ga signal due to low concentration and low thickness in a reasonable counting time (80 s for Ga, 10 for Fe and 20 for Bi). Probe size was set to 20 μm lateral defocus to minimize possible electron damage during long time and high current density analysis. Elements of the LSMO bottom electrode and of the STO substrate were also measured. Mass thickness (*ρ.e*) and composition of the LSMO and STO were fixed in the TFA program. Mass thickness and composition of the BGFO-*x* top layer was simultaneously computed by the TFA program to fit the

experimental *k*-ratio measurement for each element. From weight percent determined by TFA/WDS analysis, atomic percent can be determined and converted into Ga content (*x*) assuming the Bi_wGa_xFe_yO_z formula with *z* = 3.

Structural characterization was realized by High Resolution X-ray diffraction (HR-XRD) with a Cu *k*α₁ parallel beam (4-circles D8 Discover, Bruker). The lateral extension of the beam footprint on the sample is controlled by the insertion of a 100 μm wide slit. Piezo-force microscopy (PFM) with a commercial scanning probe microscope (Dimension 3100, Bruker) in contact mode was used to study the polar domains configuration and the piezoelectric response of the film with sub-micron resolution. For local effective piezoelectric coefficient (*d*₃₃^{eff}) measurements, an AC voltage (6 V at 15 kHz) was applied to the sample, while a DC bias (-4 V to 5 V) was applied to the tip (Pt coated tip with a spring constant of 40 N/m and resonance frequency of around 300 kHz) for complete reversal loop. Imaging of the polar domains was performed using a Co/Cr coated tip with a spring constant of 2 N/m. Piezoelectric characterizations were also made at higher length scale on 30 × 30 μm² top Pt electrodes (dc-sputter deposited via a lift-off process) using a laser scanning vibrometer (LSV model MSA-500, Polytec). In order to reduce substrate deformation during measurement, the sample was glued on a metal plate. A differential measurement between two laser beams positioned on top and outside of the Pt electrode, respectively, allows for the subtraction of the residual substrate movement from the surface displacement.³³ An AC excitation of 1 V at 100 kHz is applied between the top and the bottom electrode while surface velocity and displacement are measured via Doppler effect detected through laser interferometry.

III. RESULTS AND DISCUSSION

The $\Theta-2\Theta$ XRD patterns recorded at various locations of a 57 nm thick composition spread BGFO film are shown in Figure 1(a) and labeled according to the nominal Ga content. All the peaks present on the XRD patterns could be indexed as (001)_{pc} pseudo cubic reflections from the films or the substrate, showing that the films are (001)_{pc} oriented. No parasitic phase could be detected as no extra peaks showed up in the XRD patterns. A zoom around the (002)_{pc} reflection of the XRD patterns is represented in Figure 1(b). We can see from that figure that the BGFO (002)_{pc} peak is shifting toward higher 2θ values upon increasing Ga content from 1% to 11%. This reflects the fact that Ga is being incorporated into the perovskite structure and that the out-of-plane lattice parameter decreases upon Ga doping. A slight shoulder appears on the right side of the BGFO (002)_{pc} peak starting from *x* = 7% pattern. For *x* = 9%, this shoulder develops into a second peak moving to higher 2Θ values together with the first peak and this trend is amplified for *x* = 11%. One possible reason for the emergence of the second peak could be strain relaxation as the STO substrate exerts a compressive stress on BFO and probably on lightly doped BGFO (*a*_{STO} = 0.3905 nm and *a*_{pcBFO} = 0.3964 nm). This would in return imply that the relaxation critical thickness in BGFO depends on Ga content as no shoulder is

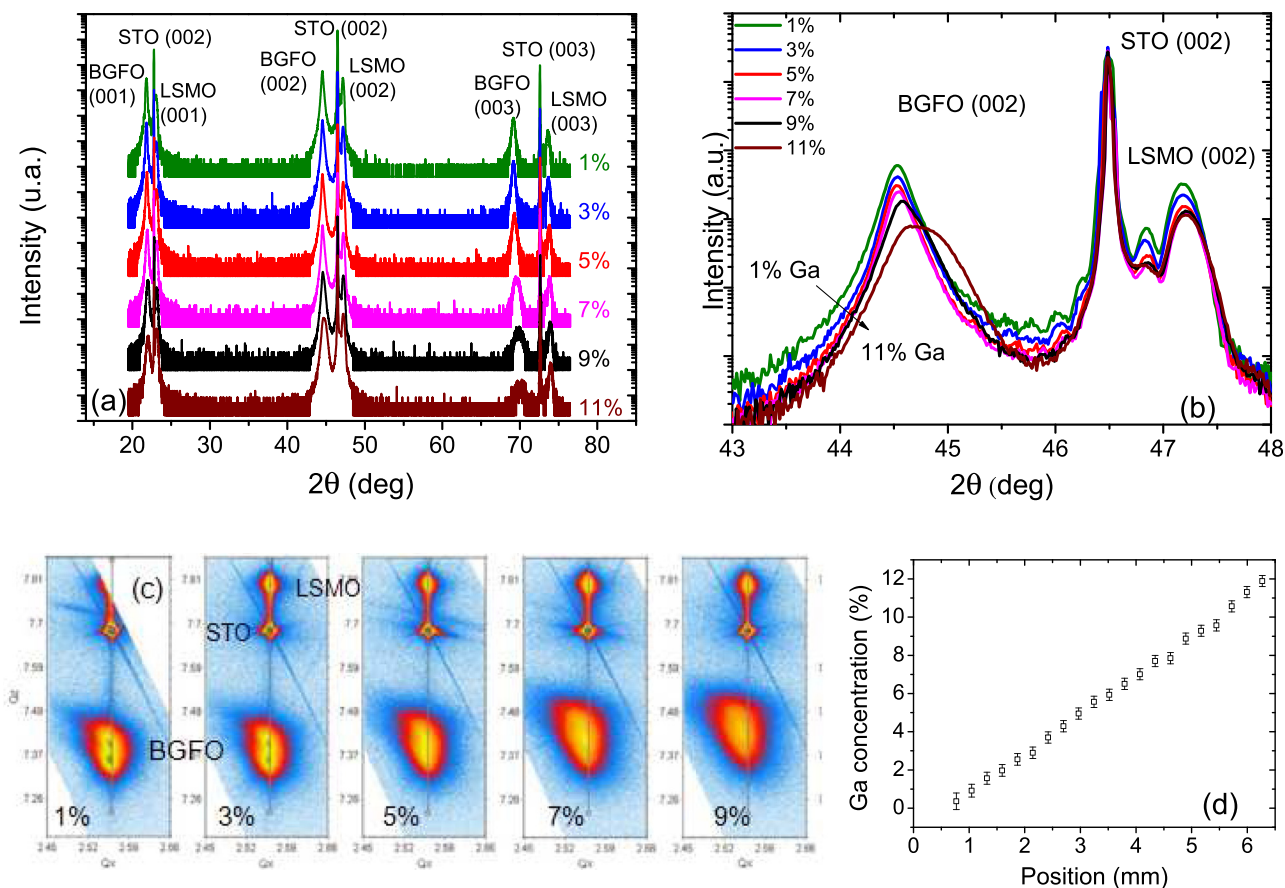


FIG. 1. (a) XRD patterns from θ - 2θ scans of BGFO- x films for $0\% \leq x \leq 11\%$. (b) Zoom around the (002) reflection. (c) Reciprocal space maps around the $(103)_{pc}$ reflections for various Ga content. (d) Ga concentration measured by WDS along the composition gradient.

observed below 6%. Another plausible reason could be a symmetry change of the BGFO film upon Ga doping, as one would expect going through an MPB.

To get more insights, reciprocal space maps (RSM) around the $(103)_{pc}$ STO reflection for various Ga doping were recorded and are presented in Figure 1(c). The RSM of BGFO $(103)_{pc}$ reflection for $x = 1\%$ displays a splitting in two peaks lying at the same Q_x but with different Q_z . A similar $(h0l)_{pc}$ splitting has already been reported for epitaxial BFO films grown on STO cubic substrate and was ascribed to BFO's symmetry lowering from rhombohedral to monoclinic (space group C_m or C_c) due to the biaxial compressive strain.³⁴ Monoclinic strained BFO with thicknesses below 100 nm also exhibit a triple splitting of the $(113)_{pc}$ reflection^{34,35} that we too have observed on pure BFO films (not shown). The splitting of BGFO- x $(103)_{pc}$ reflection is present for $x = 3\%$ (Figure 1(c)), while it is barely visible for $x = 5\%$ and absent for $x \geq 7\%$. The monoclinic distortion thus decreases upon Ga doping and is undetectable for $x \geq 7\%$, i.e., a change of symmetry is occurring between 5% and 7%. This might be a signature of an MPB, and further work is required (e.g., TEM analysis) to identify the symmetry of the new phase.

TABLE I. Cationic contents w , x , and y extracted from WDX assuming the formula $Bi_wGa_xFe_yO_3$.

w (Bi)	1.001	0.989	0.987	0.992	0.988	0.976	0.967	0.948	0.931	0.922	0.895	0.878
x (Ga) $\times 100$	0.0	1.0	1.9	2.9	4.0	5.2	6.2	7.2	8.0	9.1	10.1	11.2
y (Fe)	0.999	1.001	0.994	0.979	0.973	0.972	0.970	0.980	0.988	0.987	1.004	1.010

WDS line analysis were done along and across the composition gradient (1 point each 300 μ m). Assuming the $Bi_wGa_xFe_yO_3$ formula with $z = 3$, cationic contents w , x , and y have been extracted and are reported in Table I. The measurement error on x , w , and y is estimated to be ± 0.005 here. We note that both Bi and Fe contents (w and y respectively) decrease from 1 for pure $BiFeO_3$ to about 0.97 for 6% Ga doping. As x increases from 6% to 12%, Fe content goes back to about 1.0 while Bi content continue to decrease. From these values, one could suspect that Ga is substituted partly for Bi and partly for Fe. A precise A site to B site occupation ratio for Ga is difficult to establish although it seems to evolve with Ga content. The extracted Ga content is plotted versus position in Figure 1(d), showing a linear increase from 0% up to 12%, in good agreement with the nominal concentrations. Furthermore, composition across the gradient remained stable, and a small thickness variation ($\pm 10\%$) was seen along the line profiles (not presented here). In parallel to the WDS measurements, a systematic study of the composition variation in our samples was realized by Rutherford Backscattering Spectroscopy experiments (to be presented in a future publication). These results confirm the WDS measured Ga content.

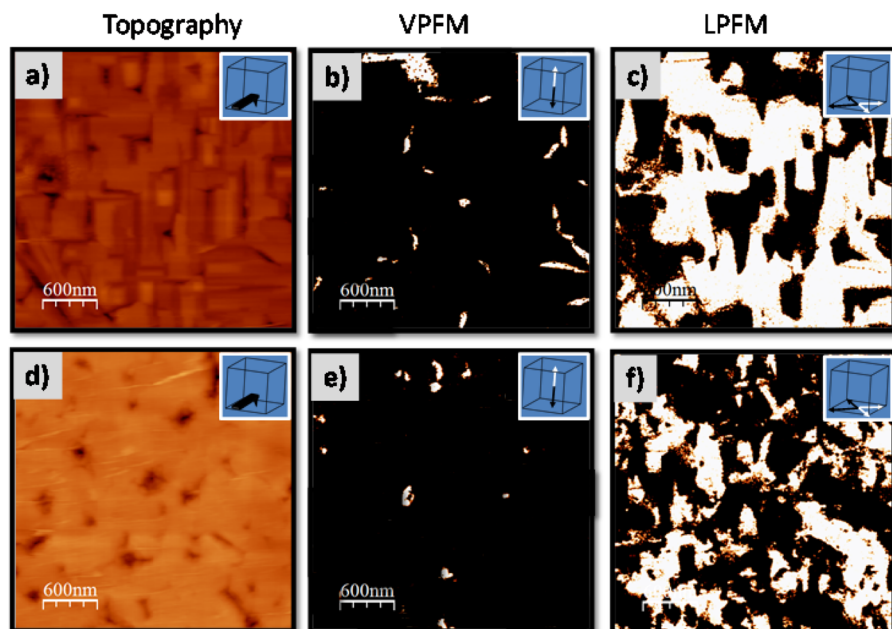


FIG. 2. Piezoresponse force microscopy images of topography (a), out-of-plane phase (b), and in-plane phase (c) for a pure BFO and corresponding topography (d), out-of-plane phase (e), and in-plane phase (f) for a $x = 6\%$.

The ferroelectric domain configuration and piezoelectric properties were then characterized on a 135 nm thick composition spread film. Figures 2(b) and 2(c) present typical in-plane (LPFM) and out-of-plane (VPFM) phase images respectively and the associated topography on a $3 \times 3 \mu\text{m}^2$ area (a) for part of the film for undoped BFO, whereas Figures 2(d)–2(f) show corresponding images for $x = 6\%$. The topography of the film changes as the amount of Ga is increased from squared-shape features to a more rounded less discernable grains. The phase contrast, indicative of different orientation of the polar domains, can be seen in both in-plane and out-of-plane phases. In addition, they present an irregular and disordered shape, characteristic of a mosaic-like domains configuration, as reported previously.^{36,37} White contrast domains are almost continuous in Fig. 2(c). The dark contrast denotes an in-plane component of the polarization pointing to the left of the cantilever while the bright contrast corresponds to an in-plane component of the polarization pointing to the right of the cantilever (LPFM Figures 2(c) and 2(f)). Knowing that the measured direction is along [100] of the STO substrate, we thus have two possible in-plane components of the polarization for each bright and dark contrasts (see the inset in Figures 2(c) and 2(f)). Namely, the bright contrast corresponds to either [11 k] or [1-1 k] directions of polarization, and the dark contrast corresponds to either [-1-1 k] or [-11 k] directions of polarization ($k = \pm 1$). For $x = 6\%$ (Figures 2(d)–2(f)), the size of the polar domains seems reduced. The white contrast domains are now dispersed and domain walls roughness increased. Considering the out-of-plane contrast (Figures 2(b) and 2(e)), it can be seen that most of the contrast is dark. This implies that most of the film as a polarization pointing downwards ($k = -1$) with very few domains showing a polarization pointing upwards ($k = +1$). The effect of Ga doping is minimal and does not affect the out-of-plane polar ground state, in terms of orientations of polarization. In order to fully establish the directions of polarization, it is necessary

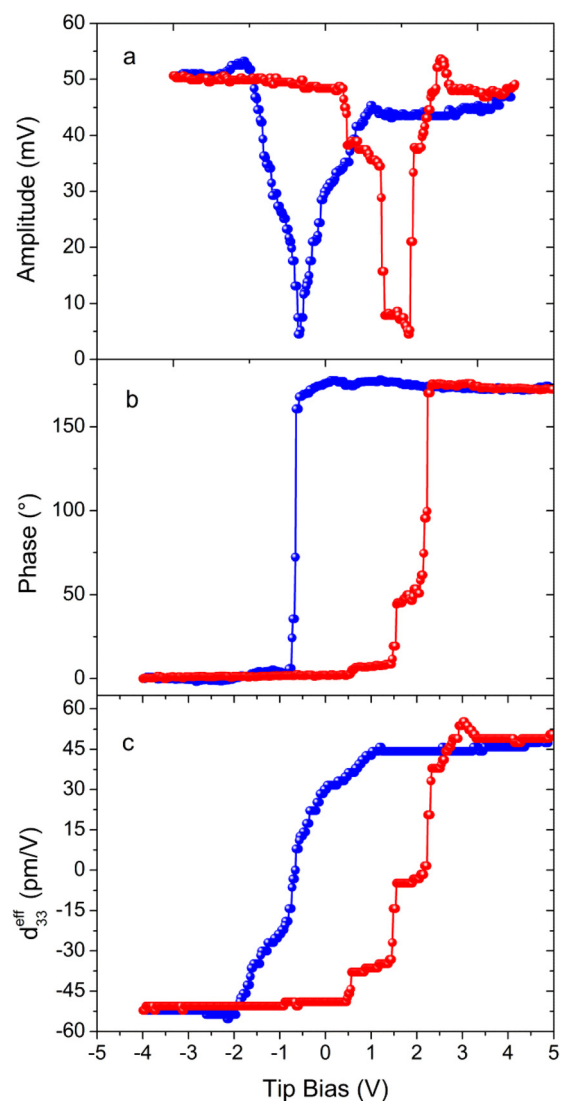


FIG. 3. Piezoresponse measurements for 5% of Ga content, Piezoresponse amplitude (a), phase (b), and effective piezoelectric coefficient (c) are shown as a function of the applied tip bias.

to take measurements at the same location by rotating the sample by 90° , but this is out of the scope of this paper.

Local piezoelectric properties of the film were measured for a few compositions. Examples of the amplitude of the piezoresponse, the phase, and d_{33}^{eff} are displayed in Figures 3(a)–3(c) for $x = 5\%$ Ga as a function of tip bias. The d_{33}^{eff} value was tentatively calculated from the measured piezoresponse amplitude taking into account the sensitivity of the photodetector (via force plot) and the out-of-plane gain. Typical ferroelectric behavior is displayed by the loops. Namely, a phase change of 180° is observed at the coercive voltage accompanied by a drop in the piezoresponse amplitude due to increasing domain wall density under the tip as the polarization switches. The reconstructed d_{33}^{eff} follows the behavior of the switched polarization (since polarization is proportional to d_{33}^{eff}) forming the classical ferroelectric hysteric loop. For the pure BFO part of the film, a d_{33}^{eff} value of ~ 15 pm/V is found while it is as high as ~ 45 pm/V for a 5% doped BGFO part of the film. We emphasize, however, that d_{33}^{eff} values extracted from PFM should be considered with caution as multiple artifact, e.g., electrostatic interactions between the cantilever and the sample, can kick in. The electrical field under the tip is not uniform either.

In order to get a systematic quantitative study of the piezoelectric properties across the composition gradient, we performed LSV measurements. Using a small laser spot size ($\sim 3 \mu\text{m}$) relative to the electrode surface ($30 \times 30 \mu\text{m}^2$), multiple LSV measurements were done on top electrodes along three lines across the composition gradient. The displacement value in each point was obtained by averaging 15 measurements. A typical mapping of the extracted d_{33}^{eff} across one electrode is presented in Figure 4(a), showing that only the area under the electrode vibrates with a uniform displacement.

Figure 4(b) shows the variation of the d_{33}^{eff} as a function of Ga content obtained with 1 V ac excitation. The error bars denote the statistical dispersion of the measurement (1σ). The d_{33}^{eff} coefficient increases upon Ga doping from 25 pm/V for pure BFO to 37 pm/V for $x = 3\%$ and then remains constant up to $x = 5.5\%$. An abrupt rise is then observed for Ga concentration above 6% followed by an abrupt fall giving a sharp peak centered just below 7%. The maximum d_{33}^{eff} value is about 53 pm/V, which is twice as large as the values obtained for undoped BFO. Finally, the fall of d_{33}^{eff} continues down to 15 pm/V for the highest Ga concentrations measured here ($x = 10\%$). The sharp enhancement of piezoelectric properties occurring around 6.5% of Ga doping is correlated

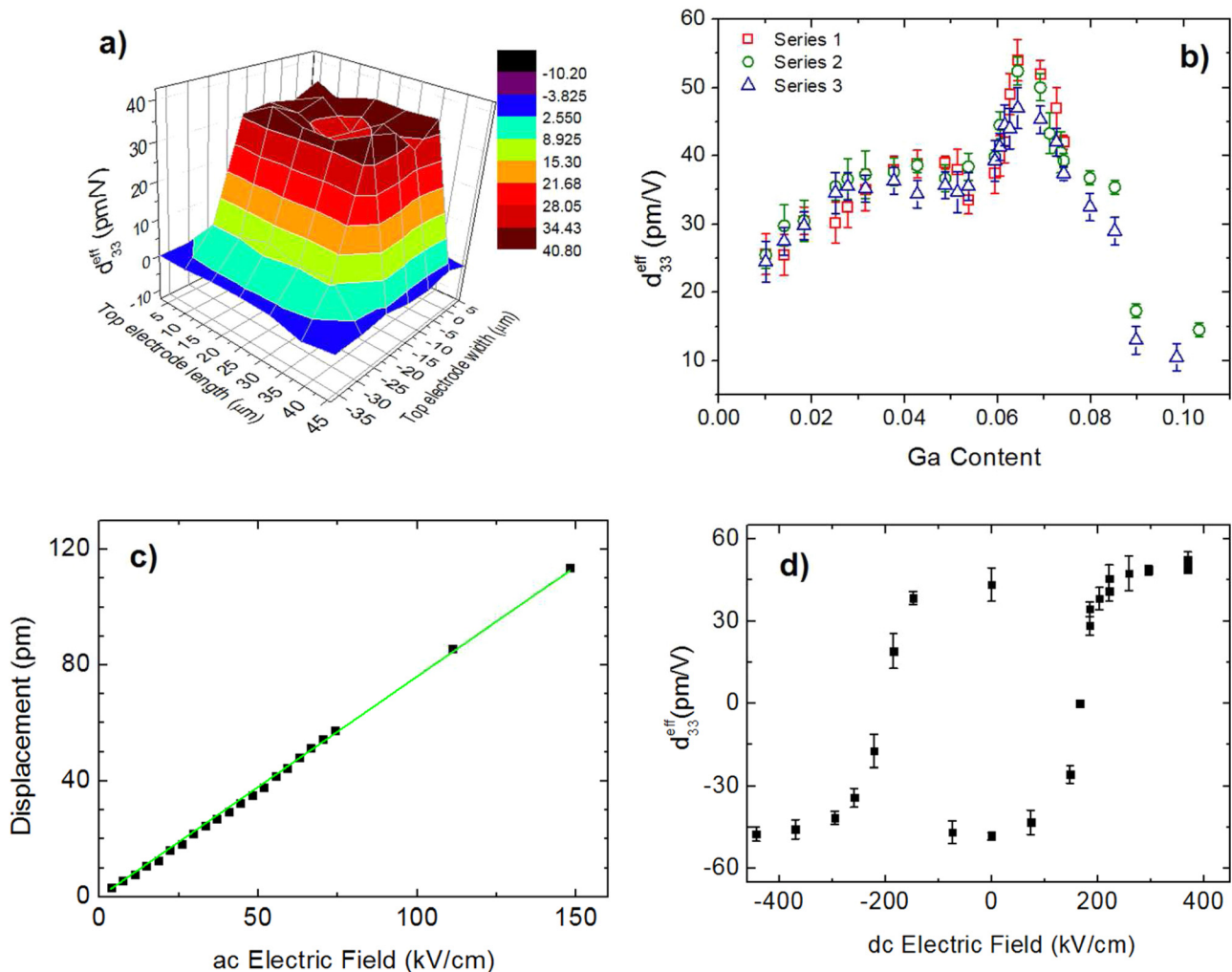


FIG. 4. (a) d_{33}^{eff} mapping of a top electrode measured by laser vibrometry. (b) d_{33}^{eff} as a function of Ga content. Displacement versus ac electric field (c) and d_{33}^{eff} versus dc electric field cycle (d) for $x = 6.5\%$.

with the symmetry change observed around the same composition and probably corresponds to the presence of a MPB.

The large d_{33} coefficients observed in bulk materials like PZT result from both intrinsic piezoelectricity and extrinsic causes dominated by ferroelastic domain rearrangement via non-180° domain wall (DW) movements. It is well known that in thin films, the corresponding d_{33}^{eff} effective coefficients are reduced and thickness dependent because of substrate clamping and DW hindered dynamic.³⁸ The maximum reported d_{33} value for bulk BFO is 40 pm/V in ceramics³⁹ while reduced d_{33} values are reported for epitaxial BFO films grown on STO: 15 pm/V for 250 nm thick film by XRD⁴⁰ and about 30 pm/V for 75 nm thick Mn-doped BFO by PFM.⁴¹ A noticeable exception to this reduced d_{33}^{eff} in film compared to bulk is reported in Ref. 42, where values of 85 pm/V (i.e., twice the best bulk value!) and 51 pm/V have been, respectively, obtained by PFM measurements for 450 nm and 135 nm thick BFO films. In polycrystalline PZT films with composition close to the MBP, a thickness well above 1 μm is necessary to obtain a d_{33}^{eff} coefficient higher than 100 pm/V, i.e., far below their bulk counterpart.^{38,43} A record d_{33}^{eff} value of 200 pm/V was obtained in epitaxial 3.8 μm thick PZT films of the same composition grown on STO substrate, while again a rapid drop below 1 μm is observed.⁴⁴

In order to compare with the results presented here, a d_{33}^{eff} of 48 pm/V can be extrapolated from Figure 4(b) of Ref. 44 for a thickness of 135 nm. For such small thicknesses, extrinsic contribution to piezoelectric coefficient is negligible in PZT.³⁸ In (001)_{pc} epitaxial BFO with monoclinic symmetry, the four polarization variants pointing upward (respectively, downward) have the same vertical component. So, upon *c* axis field excitation, all four ferroelectric domains are energetically equivalent and there is no driving force for domain wall contribution to piezoelectric effect. While this is probably the case for BGFO-*x* films up to 5%, this is not necessarily true for higher Ga content with the symmetry change. To investigate on an eventual extrinsic contribution, we measured the ac electric field dependence of the vertical displacement. A linear variation of the measured displacement is observed up to an ac field of 150 kV/cm as exemplified in Figure 4(c) for *x* = 6.5% and a d_{33}^{eff} of 55 pm/V can be extracted from the slope for a BGFO film thickness of 135 nm. This confirms the absence of extrinsic contribution via DW motion up to 150 kV/cm. Another indication of hindered DW motion can be seen from the d_{33}^{eff} dependence upon dc electric field loop (Figure 4(d)), where a coercive field of about 175 kV/cm reflects a hard piezoelectric behavior. So, the peak value of 55 pm/V for *x* = 6.5% is purely intrinsic and compare advantageously to the best epitaxial PZT value reported for the same thickness.

IV. CONCLUSION

In conclusion, we synthesized composition spread $\text{Bi}_{1-x}\text{Ga}_x\text{FeO}_3$ epitaxial thin films. All compositions were found to exhibit typical hysteretic ferroelectric behavior with a slight reduction of ferroelectric domain sizes upon Ga doping. A change of symmetry has been evidenced between 5% and 7% of Ga doping and is correlated with a sharp

enhancement of the effective piezoelectric coefficient (two-fold increase compared to pure BFO) for 6.5% of Ga which probably results from the presence of a morphotropic phase boundary at this composition. The d_{33}^{eff} maximum (55 pm/V for a thickness of 135 nm) shows no extrinsic domain wall contribution and compares to the best reported PZT value for the same thickness.

ACKNOWLEDGMENTS

This work was funded by Région Centre in the frame of the project Oxymore.

- ¹S. Trolier-McKinstry and P. Muralt, *J. Electroceram.* **12**, 7 (2004).
- ²M. Davis, *J. Electroceram.* **19**, 25 (2007).
- ³B. Jaffe, W. R. Cook, and H. Jaffe, *Piezoelectric Ceramics* (Academic, London, 1971), p. 136.
- ⁴T. Shrout, Z. Chang, N. Kim, and S. Markgraf, *Ferroelectr., Lett. Sect.* **12**, 63 (1990).
- ⁵M. Ahart, M. Somayazulu, R. E. Cohen, P. Ganesh, P. Dera, H.-K. Mao, R. J. Hemley, Y. Ren, P. Liermann, and Z. Wu, *Nature* **451**, 545 (2008).
- ⁶B. Noheda, D. E. Cox, G. Shirane, J. A. Gonzalo, L. E. Cross, and S. E. Park, *Phys. Rev. Lett.* **86**, 3891 (2001).
- ⁷B. Noheda, D. E. Cox, G. Shirane, J. A. Gonzalo, L. E. Cross, and S.-E. Park, *Appl. Phys. Lett.* **74**, 2059 (1999).
- ⁸W. Kaczmarek and Z. Pajak, *Solid State Commun.* **17**, 807 (1975).
- ⁹Y. E. Roginskaya, Y. Y. Tomoshpolskii, Y. N. Venevstev, V. M. Petrov, and G. S. Zhdanov, *Sov. Phys.-JETP* **23**, 47 (1966).
- ¹⁰F. Kubel and H. Schmid, *Acta Crystallogr. B* **B46**, 698 (1990).
- ¹¹C. Michel, J.-M. Moreau, G. D. Achenbechi, R. Gerson, and W. J. James, *Solid State Commun.* **7**, 701 (1969).
- ¹²G. A. Smolenskii and V. M. Yudin, *Sov. Phys. Solid. State* **6**, 2936 (1965).
- ¹³G. Catalan and J. F. Scott, *Adv. Mater.* **21**, 2463 (2009).
- ¹⁴Y. Wei, X. Wang, J. Zhu, X. Wang, and J. Jia, *J. Am. Ceram. Soc.* **96**, 3163 (2013).
- ¹⁵D. I. Woodward, I. M. Reaney, R. E. Eitel, and C. A. Randall, *J. Appl. Phys.* **94**, 3313 (2003).
- ¹⁶V. Freitas and I. Santos, *J. Am. Ceram. Soc.* **94**, 754 (2011).
- ¹⁷R. J. Zeches, M. D. Rossell, J. X. Zhang, A. J. Hatt, Q. He, C.-H. Yang, A. Kumar, C. H. Wang, A. Melville, C. Adamo, G. Sheng, Y.-H. Chu, J. F. Ihlefeld, R. Erni, C. Ederer, V. Gopalan, L. Q. Chen, D. G. Schlom, N. A. Spaldin, L. W. Martin, and R. Ramesh, *Science* **326**, 977 (2009).
- ¹⁸F. Bai, N. Wang, J. Li, D. Viehland, P. M. Gehring, G. Xu, and G. Shirane, *J. Appl. Phys.* **96**, 1620 (2004).
- ¹⁹J. X. Zhang, B. Xiang, Q. He, J. Seidel, R. J. Zeches, P. Yu, S. Y. Yang, C. H. Wang, Y.-H. Chu, L. W. Martin, A. M. Minor, and R. Ramesh, *Nat. Nanotechnol.* **6**, 98 (2011).
- ²⁰Z. Chen, Z. Luo, C. Huang, Y. Qi, P. Yang, L. You, C. Hu, T. Wu, J. Wang, C. Gao, T. Sritharan, and L. Chen, *Adv. Funct. Mater.* **21**, 133 (2011).
- ²¹D. Kan, L. Pálóvá, V. Anbusathaiah, C. J. Cheng, S. Fujino, V. Nagarajan, K. M. Rabe, and I. Takeuchi, *Adv. Funct. Mater.* **20**, 1108 (2010).
- ²²S. Fujino, M. Murakami, V. Anbusathaiah, S. H. Lim, V. Nagarajan, C. J. Fennie, M. Wuttig, L. Salamnaca-Riba, and I. Takeuchi, *Appl. Phys. Lett.* **92**, 202904 (2008).
- ²³A. A. Belik, D. A. Rusakov, T. Furubayashi, and E. Takayama-Muromachi, *Chem. Mater.* **24**, 3056 (2012).
- ²⁴J. Yan, M. Gomi, T. Yokota, and H. Song, *Appl. Phys. Lett.* **102**, 222906 (2013).
- ²⁵Z. Fan, J. Xiao, H. Liu, P. Yang, Q. Ke, W. Ji, K. Yao, K. P. Ong, K. Zeng, and J. Wang, *ACS Appl. Mater. Interfaces* **7**, 2648 (2015).
- ²⁶G. Liu, J. Wolfman, C. Autret-Lambert, J. Sakai, S. Roger, M. Gervais, and F. Gervais, *J. Appl. Phys.* **108**, 114108 (2010).
- ²⁷S. C. Abrahams, J. M. Reddy, and J. L. Bernstein, *J. Chem. Phys.* **42**, 3957 (1965).
- ²⁸J. P. Remeika, *J. Appl. Phys.* **31**, S263 (1960).
- ²⁹B. F. Levine, C. H. Nowlin, and R. V. Jones, *Phys. Rev.* **174**, 571 (1968).
- ³⁰R. Saha, A. Shireen, S. N. Shirodkar, U. V. Waghmare, A. Sundaresan, and C. N. R. Rao, *Solid State Commun.* **152**, 1964 (2012).
- ³¹A. Belik and W. Yi, *J. Phys.: Condens. Matter* **26**, 163201 (2014).

- ³²D. P. Norton, B. C. Chakoumakos, J. Budai, D. H. Lowndes, B. C. Sales, J. R. Thompson, and D. K. Christen, *Science* **265**, 2074 (1994).
- ³³A. L. Kholkin, C. Wutchrich, D. V. Taylor, and N. Setter, *Rev. Sci. Instrum.* **67**, 1935 (1996).
- ³⁴F. L. Marrec, H. Toupet, C. Lichtensteiger, B. Dkhilc, and M. Karkut, *Phase Transitions* **84**, 453 (2011).
- ³⁵C. M. Daumont, S. Farokhipoor, A. Ferri, J. C. Wodjel, J. Íñiguez, B. J. Kooi, and B. Noheda, *Phys. Rev. B* **81**, 144115 (2010).
- ³⁶G. Catalan, H. Béa, S. Fusil, M. Bibes, P. Paruch, A. Barthélémy, and J. Scott, *Phys. Rev. Lett.* **100**, 027602 (2008).
- ³⁷L. Martin, Y.-H. Chu, M. Holcomb, M. Huijben, P. Yu, S.-J. Han, D. Lee, S. Wang, and R. Ramesh, *Nano Lett.* **8**, 2050 (2008).
- ³⁸F. Xu, S. Trolier-McKinstry, W. Ren, B. Xu, Z.-L. Xie, and K. J. Hemker, *J. Appl. Phys.* **89**, 1336 (2001).
- ³⁹T. Rojac, A. Bencan, G. Drazic, M. Kosec, and D. Damjanovic, *J. Appl. Phys.* **112**, 064114 (2012).
- ⁴⁰C. W. Bark, S. Ryu, Y. M. Koo, H. M. Jang, and H. S. Youn, *Appl. Phys. Lett.* **90**, 022902 (2007).
- ⁴¹C. Daumont *et al.*, *J. Phys.: Condens. Matter* **24**, 162202 (2012).
- ⁴²J. Wang *et al.*, *Science* **299**, 1719 (2003).
- ⁴³N. Lederemann, P. Muralt, J. Baborowski, S. Gentil, and K. Mukati, *Sens. Actuators, A* **105**, 162 (2003).
- ⁴⁴D. M. Kim, C. B. Eom, V. Nagarajan, J. Ouyang, R. Ramesh, V. Vaithyanathan, and D. G. Schlom, *Appl. Phys. Lett.* **88**, 142904 (2006).